JOURNAL OF MATERIALS SCIENCE: MATERIALS IN MEDICINE **16** (2005) 197–202

Corrosion testing of sintered samples made of the Co-Cr-Mo alloy for surgical applications

E. KRASICKA-CYDZIK[1], Z. OKSIUTA[2], J. R. DABROWSKI[2]
[1]*University of Zielona Gora, Poland*
[2]*Technical University of Bialystok, Poland*

Corrosion resistance of high quality sintered compacts made of the Co-Cr-Mo alloy powder in manufacturing bone implants has been investigated. The samples met the characteristic mechanical requirements for this kind of implants, but the increased density of the porous material turned out to be crucial in the improvement of their corrosion resistance. It seems that the rotary cold repressing (RCR) of sintered compacts could be a very advantageous alternative to the single or multiple matrix pressing. The influence of cold repressing and the subsequent heat treatment of sintered compacts made of the Co-Cr-Mo powder on the changes of their density, microstructure, and corrosion resistance was investigated in this work.

1. Introduction

The behavior of implant materials in the tissue environment is a key factor in their application in surgery. Corrosion of metals and their alloys can significantly influence the meta-stable equilibrium of the tissue/implant interface. It finally leads to negative toxic reactions such as: osteolysis, infections, or metabolic changes [1, 2]. Both the type and the intensity of corrosion depend on the chemical composition of the material, structure homogeneities, the features of the geometrical implant as well as different connected factors, e.g., production technology.

Due to the proper corrosion resistance and mechanical properties, the Co-Cr-Mo alloy, also known as Vitalium, is one of the most popular metallic materials used in implantology practice. Its corrosion resistance in human body is better than the one for stainless steel (AISI 316L) but worse than the values for titanium alloys.

Many works [3–5] have reported that porous metallic materials are characterized by worse corrosion resistance in comparison with their fully dense cast or wrought equivalents. It is due to their lower densities and the increased real surface area. Studies [4, 5] have showed that the corrosion behaviour of porous metallic materials, particularly in case of the crevice corrosion, are also influenced by the pores morphology and the internal surface area.

It is well known [3–6] that, beside the temperatures and time of sintering, the kind of sintering atmosphere apparently influences the corrosion resistance of porous sintered samples. Various sintering atmospheres have different influence on the structure of porous materials. The best corrosion properties characterize the Co-Cr-Mo samples sintered in the argon atmosphere [3, 4]. The flowing molecular atmosphere $75H_2$–$25N_2$ (75 wt% H_2–25 wt% N_2) appears to precipitate Cr_2N, which reduces the corrosion resistance (break down of the passive oxide film) of the sintered Co-Cr-Mo specimens. The vacuum sintering induces, especially in the surface layers of the specimens, chromium loss by volatilization and also carbon loss owing to the decarburisation. Also the atomic absorption analysis of the amount of ions dissolved in the corrosion test solutions showed [3] that the largest concentration of toxic elements was observed in the case of the vacuum sintered specimens.

It was found [4] that severe crevice corrosion in the case of the sintered Co-Cr-Mo samples corresponds to the total pore volume fraction ranging from 17 to 20%. It should be emphasized that, with regard to the corrosion resistance of the sintered materials, not only porosity, but also the size and shape of the pores are important factors. It has been suggested [3, 5] that small pores of a globular shape are better than narrow, elongated ones.

This work aims at determining the influence of the stages of the technological process (sintering, rotary cold repressing, and heat treatment) on the corrosion resistance of the porous Co-Cr-Mo alloy samples.

2. Materials and methods

The powder alloy was produced by applying the water atomisation method to the cast Co-Cr-Mo alloy (ISO 5832–4) with the particle size distribution of $20 \div 200$ μm. The sintering powder was annealed in dry hydrogen at 1000 °C for 2 h before the process. The chemical analysis of the Co-Cr-Mo alloy powder after annealing in the hydrogen atmosphere is given in Table I. After compaction at the pressure of 600 MPa, the samples were sintered under the argon atmosphere at the temperature of 1250 °C for 1 h. The specimens were cooled down naturally to the ambient temperature inside the furnace. The rotary cold repressing was

TABLE I Chemical composition of Co-Cr-Mo alloy (wt%)

C	O	Mo	Si	P	Ni	Fe	S	Cr	W	Co
0.31	0.57	5.40	0.50	0.01	0.02	1.37	0.01	29.29	0.01	Bal.

TABLE II Samples for corrosion tests

Sample	Sample preparation
K0	Cast Co-Cr-Mo alloy
K1	Sintered Co-Cr-Mo alloy at 1250 °C, in argon, for 1 h
K2	K1 + Rotary cold repressed sample ($\tau = 5$ s, $p = 600$ MPa)
K3	K2 + Heat treated (saturated) sample at 1250 °C, in argon, for 1 h
K4	Classical double sintered and repressed sample

performed with a PXW 100A press at 600 MPa, using $i = 12$ rotations. After repressing, the samples were heat treated at the temperature of 1250 °C for 1 h in dry argon and then cooled down at the average speed of 45 ° C/min. The samples structure was examined with an optical microscope (Neophot 21) and a scanning electron microscope (Hitachi 3000N) with an X-ray microanalyser. The cast Co-Cr-Mo and classical double sintered as well as cold compacted specimens were used for comparison. The samples prepared for the corrosion investigations are described in Table II.

Before the corrosion tests were carried out, cylindrical samples of 8 mm in diameter and 8 mm in length were ground, mechanically polished and ultrasonically washed in a double-distillated water. The lateral surfaces of the specimens were covered by insulating lacquer in order to expose only $0.505 \div 0.525$ cm^2 of cross section area of the samples to the testing solution. The electrochemical behaviour of the samples was evaluated on the basis of the potentiodynamic polarization curves, according to the ISO specification [7–9]. The experiments with ATLAS 9833 Electrochemical Interface (Poland) were performed in a 1000 cm^3 glass cell using the Ringer/s solution at 37 ± 0.5 °C as the electrolyte, the platinum foil (10 cm^2) as the counter and the saturated calomel electrode (SCE) as the reference.

3. Results and discussion

The specimens sintered in the argon atmosphere of the relative density $68 \div 70\%$ show the structure presented in Fig. 1 [6, 10], which consists of a fine grained solid

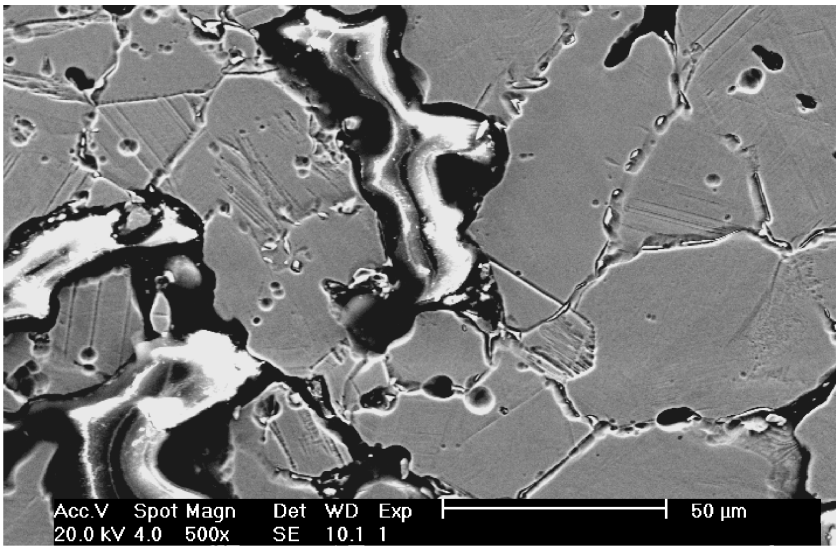

(a)

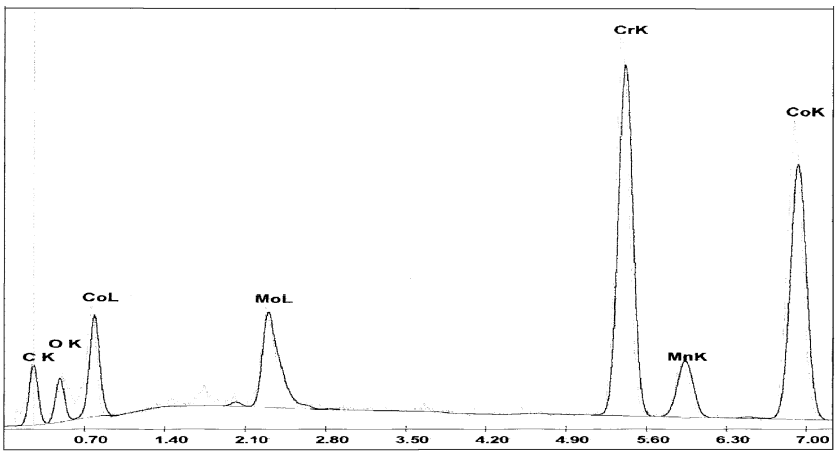

(b)

Figure 1 The analysis of the sintered samples: (a) SEM microstructure and (b) X-ray microanalysis of the precipitations.

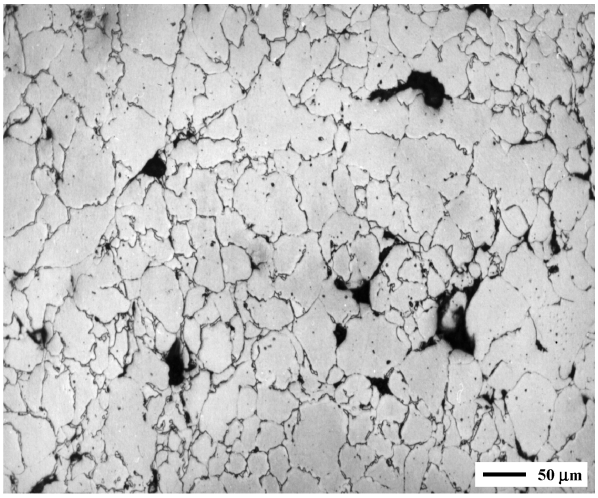

(a)

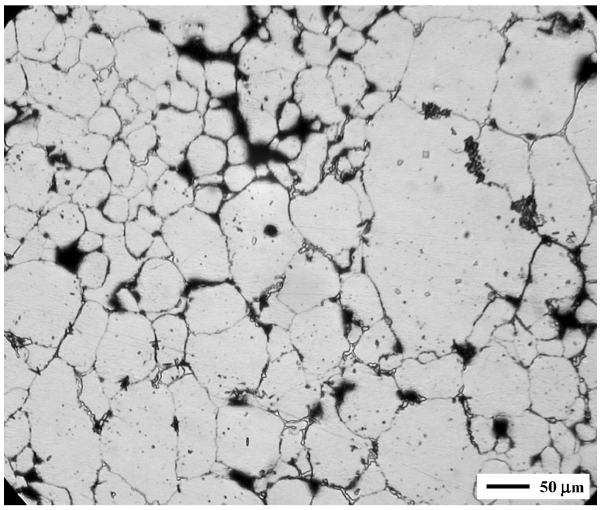

(b)

Figure 2 The samples microstructure: (a) after repressing $p = 600$ MPa, $i = 12$ rotations and (b) after heat treatment at 1250 °C for 1 h in argon.

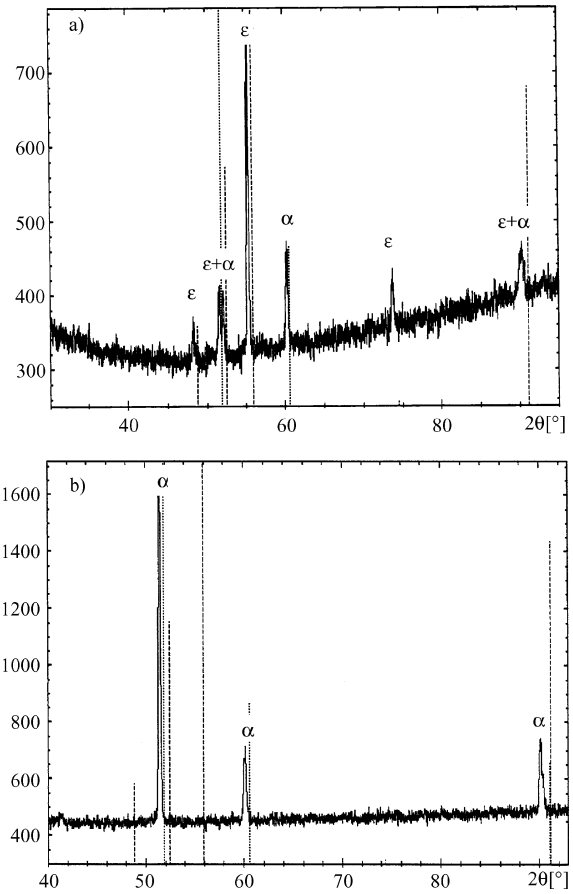

Figure 3 Diffraction patterns of the sintered samples: (a) repressed and (b) heat treated.

solution of chromium, molybdenum and carbon in α-Co with some precipitations of the second phase as well as carbides and oxides particles, located mainly along the grain boundaries. The results of a chemical microanalysis show a homogeneous arrangement of the basic alloying elements (chromium and molybdenum) in the solid solution [6].

The rotary cold repressing increased the relative density of the samples to $86 \div 88\%$. Fig. 2(a) displays the structure of the samples after repressing. As a result of the plastic deformation, the fcc – hcp ε-martensitic phase change was observed (Fig. 3).

The subsequent heat treatment carried out after the repressing did not change significantly the samples density, the grain sizes (Fig. 2(b)), or the distribution of the main alloying elements within the metallic matrix. The cobalt α-phase appeared only to be present in the heat-treated specimens (Fig. 3(b)) analysed by the X-ray diffraction.

The structure and porosity of the materials obtained during the subsequent stages of the PM process [11] showed to have a significant influence on the corrosion resistance of the investigated samples. The examples of polarization curves, within the potential range from E_{cor} to 1.5 V vs. the saturated calomel electrode (SCE) are shown in Figs. 4 and 5. In Table III, the values of the electrochemical parameters are listed.

The values of the corrosion potential E_{cor} and the repassivation potentials E_{rep} determined by the balance between the anodic and cathodic reactions of any investigated material in the Ringer's solution depend on the surface energy of the specimens after the mechanical shaping and surface treatment processes [12].

Table III and Fig. 4(a) show the lowest value of the corrosion potential E_{cor} and a typical anodic

TABLE III Corrosion E_{cor} and repassivation E_{rep} potentials and passive current densities i_{pass} for sintered Co-Cr-Mo samples in Ringer's solution (SCE)

Sample	Porosity (%)	E_{cor} (mV)	E_{rep} (mV)	i_{pass} (μA/cm^2)	log i_{pass} (μA/cm^2)
K0	–	$-185 \div -175$	$+5 \div 28$	$1.9 \div 4.8$	$0.30 \div 0.68$
K1	32.0	$-54 \div -30$	$+120 \div 176$	$354 \div 371$	$2.43 \div 2.48$
K2	13.5	$-30 \div -25$	$+248 \div 298$	$269 \div 301$	$2.55 \div 2.57$
K3	12.2	$+20 \div +23$	$+105 \div 132$	$51 \div 154$	$1.71 \div 2.19$
K4	19.0	$+21 \div +74$	$+338 \div 394$	$89 \div 115$	$1.95 \div 2.06$

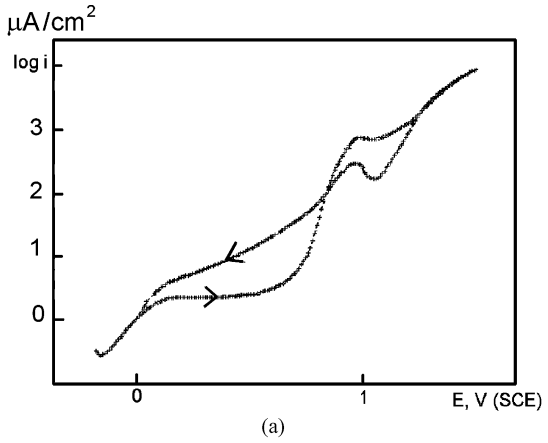

(a)

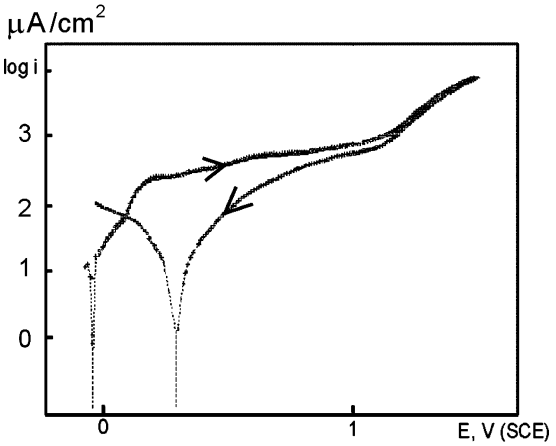

(b)

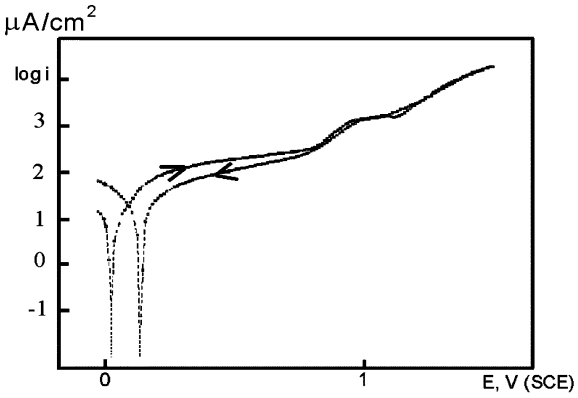

(c)

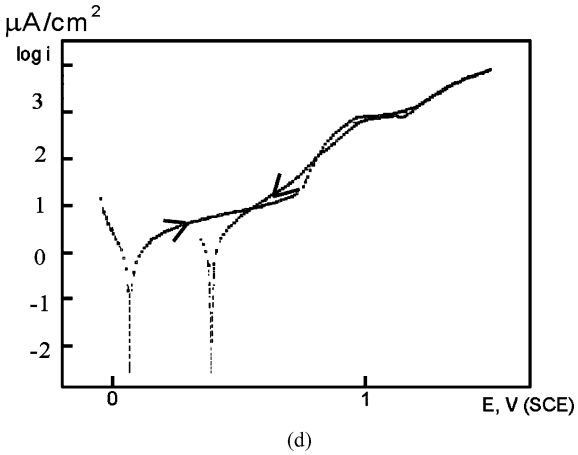

(d)

Figure 4 Examples of polarization curves of potential versus current for specimens: (a) Cast Vitalium, K0, (b) sintered cobalt alloy samples K1, (c) re-pressed specimens, K2 and (d) re-pressed specimens with the additional heat treatment, K3.

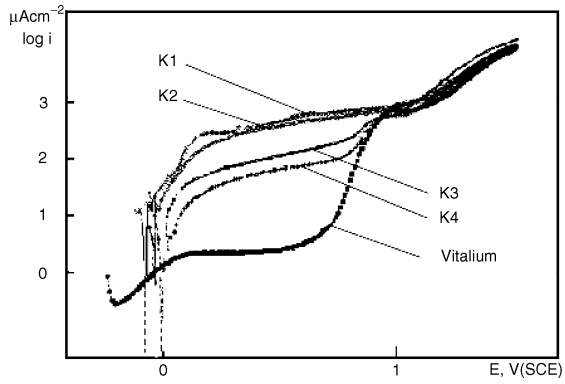

Figure 5 The comparison of the polarization curves for Vitalium and the sintered Co-Cr-Mo alloy specimens, K1—sintered sample, K2—rotary cold repressed sample, K3—repressed specimens additionally heat-treated, K4—classical sintered and repressed sample.

polarization curve with a low passive current density (3.5×10^{-2} Am^{-2}) for the Vitalium samples. At the potential higher than +0.8 V (SCE), the potentiodynamic curve shows a peak which, basing on [13], can be attributed to the transpassive oxidation of Cr^{3+} to Cr^{6+} according to the following reaction:

$$3Cr^{3+} + 4H_2O \rightarrow Cr_2O_3 + 6H^+ + 6e^- \qquad (1)$$

The described peak precedes the large current rise due to the onset of H_2O oxidation. In the potential range to 1.5 V (SCE), neither a rapid increase in the current density during the forward scan (except that caused by the oxygen evolution) nor a hysteresis loop were observed. A small peak on the reverse scan of the voltammogram is thought to appear due to the reduction of oxide, formed previously on the Vitalium during the forward scan. However upon reversing the scan, the reduction wave show reduced intensity, but the current density in the passive region is higher. Thus, the Vitalium seems to undergo apparent oxidation in the Ringer's solution.

As opposed to the Vitalium (Fig. 4(a)), the sintered specimens of the Co-Cr-Mo alloy do not show ideal passive behaviour and a current plateau in the passive region in the anodic polarisation curves (Fig. 4(b)–(d)). Moreover, the data in Table III indicate that the sintered specimens of the Co-Cr-Mo alloy have higher passive current densities in the passive range and higher values of the corrosion potential E_{cor} than for the cast Vitalium in the passive region. The shift of the corrosion potential E_{cor} towards the anodic direction can be caused by two factors: the higher surface energy of the material compacted under the high pressure, which is a characteristic feature of such specimens [2, 14], and the evidence of the surface layer oxidation independent of the time of exposure to the electrolyte and hence of the increased protectiveness of the oxide film due to its thickening. It is interesting that to note that the current densities for the sintered samples during the reverse scan are lower, which once again supports further growth of oxide layer on their surface. In a normal passive condition, the more noble corrosion potentials E_{cor} of the materials and the lower current densities, the better their corrosion resistance. The surface finishing

processes, i.e., re-pressing and heat treatment in case of each additional treatment, increased the corrosion potential values E_{cor} of the sintered specimens by further about 20 mV. One of the factors responsible for the changes observed on the polarization curves may be the lack of the oxidation peak at 0.8 V (SCE) on every polarization curve for the sintered samples, which confirm the presence of a stable protective oxide film on the surfaces of the sintered porous samples.

The increase of the passive current densities for the sintered samples corresponds to their expected bigger surface areas in comparison to the cast Vitalium sample. However, further analysis of the data in Table III and Fig. 4(d) reveals that both additional treatments, i.e., the re-pressing and the subsequent heat treatment, apparently decrease the passive currents to the values of $2.69 \div 3.01\ Am^{-2}$ (K2) and $0.51 \div 1.54\ Am^{-2}$ (K3), respectively.

Moreover, the values of the repassivation potentials E_{rep}, obtained on the reversed scan, are more positive than their respective forward scan values, and the bigger difference enlarges the protection potential region ($E_{prot} = E_{rep} - E_{cor}$). The latter reflects the formation of a stable passive layer and indicates the increase in the oxide layer thickness during the anodic polarization of the samples. The data in Table III shows that the lower value of the repassivation potential, $E_{rep} = 120 \div 176$ mV (SCE) was observed in the case of the sintered samples (K1) in comparison to the sintered and re-pressed specimens E_{rep} $248 \div 298$ mV (SCE) (K2). A possible explanation, deduced from a porous electrode model [15], suggests that the increase of E_{rep} may be a consequence of a beneficial change of the pores number and shape, as it was previously determined in the porosity measurements (Table III). The other reason of the increase of E_{rep} after the re-pressing process is that some pores might have been blocked during the compaction, and the E_{rep} value became only dependent on the thick oxide layer outside the pores and should thus be more positive [16]. The observed change of the porosity distribution, and the apparent decrease of the number of large pores into which the electrolyte penetrates, suggest that both hypotheses can be true.

The lowest values of the passive current density (Fig. 4(d)) were observed for the specimens which were re-pressed and heat treated. As a consequence of the applied heat treatment, the hexagonal cobalt phase was not observed in the re-pressed specimens, which became again one-phase material samples with the improved surface layer structure. This confirms explicitly that these specimens show the highest corrosion resistance among the other sintered samples. The highest corrosion resistance of the re-pressed and additionally heat treated specimens, among the other sintered specimens, is successfully proved by the fact that their current density is lower than about $1.5\ Am^{-2}$(K3).

The significant influence of the applied treatments on the improvement of the corrosion resistance of the sintered Co-Cr-Mo alloy samples in the Ringer's solution is confirmed by the comparison of the anodic polarization curves for all specimens in Figs. 5–6.

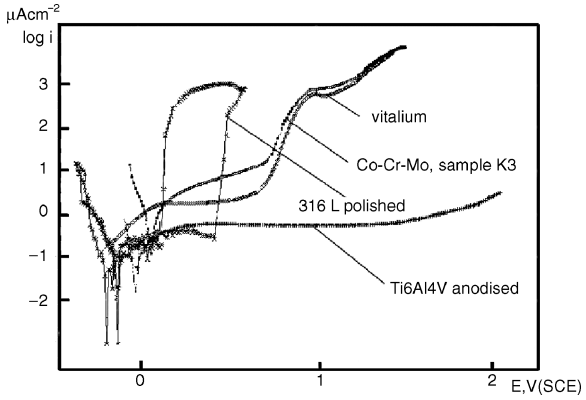

Figure 6 The polarization curves for the rotary cold re-pressed specimen of the Co-Cr-Mo alloy, additionally heat-treated—sample K3, the mechanically polished 316 L implant steel sample [17] and the Ti6Al4V alloy sample anodised in 0.5 M H_3PO_4 [18].

Although the curves in Fig. 5 indicate that the sintered specimens show a slow increase of the passive current in the passivity region, the values of the current density do not exceed the corresponding values for the Vitalium specimen at $\sim +1.0$ V (SCE) at the higher potential. In a wide potential region, up to about +0.8 V (SCE), the sample K3 (Fig. 6) shows passive behaviour similarly to the Vitalium, whereas the polished specimen of 316 L implant steel reveals a breakdown at the potential of about +0.48 V (SCE). Although higher than that for titanium and its alloys [17,18] (Fig. 6), the current densities of all sintered Co-Cr-Mo alloys within the potentials up to +0.8 V (SCE) do not exceed the value of $10\ Am^{-2}$, acceptable for passive materials [14, 15], and correspond to true values of the electrochemical potentials of metallic biomaterials, when implanted in human body.

4. Summary

The re-pressing and subsequent heat treatment applied to the sintered specimens made of the Co-Cr-Mo alloy powder influenced significantly and beneficially their micro-structure, porosity and corrosion resistance. The applied processes caused homogenizing of the alloys phase and the decrease of porosity. The increased number of medium size and small pores as well as their spheroidizing caused the improvement of the corrosion resistance of the porous sintered specimens. The highest corrosion resistance of the sintered specimens, which were additionally re-pressed and heat treated proved successfully their usefulness as biomaterials.

Acknowledgments

The support of the State Committee for Scientific Research (KBN) No. 7 T08D 03021 is gratefully acknowledged.

References

1. S. STEINEMANN, "Corrosion of Implant Alloys. Technical Principles, Design and Safety of Joint Implants" (Hogrefe & Huber Publ., Seattle-Toronto-Bern-Göttingen, 1990).

2. E. CLARKE and J. HICKMAN, *J. Bone Jt. Surg.* **35A** (1983).
3. B. S. BECKER and J. D. BOLTON, *Powder Met.* **4** (1995) 305.
4. *Idem.*, The Fifth World Biomaterials Congress, Toronto, Canada (1996) p. 475.
5. K. H. W. SEAH, R. THAMPURAN and S. H. TEOH, *Corr. Sci.* **40**(4/5) (1998) 547.
6. J. R. DĄBROWSKI, J. FRYDRYCH, H. FRYDRYCH and W. RATUSZEK, *Arch. Metall.* **46**(1) (2001) 81.
7. ASTM G3–87, Standard Reference Test Method for Making Potentiostatic and Potentiodynamic Anodic Polarization Measurements.
8. ASTM G 59–91, Standard Practice for Conducting Potentiodynamic Polarization Resistance Measurements.
9. ASTM G 61–86, Standard Test Method for Conducting Cyclic and Potentiodynamic Polarization Measurements for Localized Corrosion Susceptibility of Iron-, Nickel-, or Cobalt-Based Alloys.
10. Z. OKSIUTA and J. R. DABROWSKI, *Powder Metall.* **45**(1) (2002) 63.
11. L. WOJNAR, J. R. DABROWSKI and Z. OKSIUTA, *Mater. Character.* **46** (2001) 221.
12. K. J. BUNDY, *Biomed. Engng.* **22** (1994) 139.
13. A. W. E. HODGSON, S. KURZ, S. VIRTANEN, V. FERVEL, C.-O. A. OLSSON and S. MISCHLER, *Electrochimica Acta* **49** (2004) 2167.
14. V. CIHAL, Intergranular Corrosion of Steels and Alloys, Elsevier, 1984.
15. N. A. HAMPSON and A. J. McNEIL, The Electrochemistry of Porous Electrodes, in Electrochemistry, edited by D. Pletcher, (A Specialist Periodical Report, Royal Soc. Chem., London, 1983) Vol. 8.
16. D. C. SILVERMAN and J. C. CARRICO, *Corrosion - NACE* **5** (1988) 280.
17. E. KRASICKA-CYDZIK and J MSTOWSKI, *Bull. Acad. Mining and Metall. Cracow, Metall. Foundry Engng.* **23** (1997) 245.
18. E. KRASICKA-CYDZIK, *Biomater. Engng. (Inżynieria Biomateriałow)* **7** (1999) 42.

Received 23 January
and accepted 12 August 2004